Optimizing Wing Lift to Drag Ratio Enhancement with Flexible-Wall Turbulence Control

Sumon.K.Sinha*
Sinhatech
3607 Lyles Drive, Oxford, MS 38655, U.S.A..

Multiple in flight sink-rate measurements of a Standard Cirrus sailplane verified 18% increase in average best glide ratio (L/D) by treating 8% of the mean aerodynamic chord of the wing upper surface with a passive Flexible Composite Surface Deturbulator tape. The periodic ridged substrate of an optimized Deturbulator mitigates turbulence producing vortices by breaking long wavelength flow induced oscillations of the flexible surface. Attenuating turbulence can be used to promote a thin nearly stagnant non-dissipative separated zone on top of the wing. When optimized this increases the effective airfoil camber while eliminating skin-friction and pressure drag. Closer examination of the sink-rate data alludes to the possibility of increasing L/D by 100% when such conditions are realized.

Nomenclature

A	=	wing planform area
A_W	=	aircraft wetted surface area
A_r	=	wing aspect ratio
AFW	=	active flexible wall transducer
C_d	=	drag coefficient ($D / (qA)$ for wing), lower case c_d represents the section drag coefficient
C_{di}	=	induced drag coefficient = $C_L^2/(e\pi A_r)$
C_{do}	=	profile or parasitic drag coefficient representing drag at zero lift
C_p	=	pressure coefficient ($(p_{static} - p_{static,\infty}) / q$)
C_f	=	Flat Plate equivalent Skin Friction Coefficient ($\tau_w/(qA_w)$)
C_L	=	lift coefficient ($L / (qA)$), lower case c_L represents the section lift coefficient
c	=	airfoil chord length
D	=	drag force
e	=	Oswald span efficiency
s	=	center to center distance between two strips
f	=	FCSD control frequency (U/s)
FCSD	=	flexible composite surface deturbulator
H	=	kinematic shape factor = δ_1/δ_2
L	=	lift force
M, Ma	=	Mach number
P	=	local static pressure
$p_{static,\infty}$	=	upstream static pressure
$p_{stag,\infty}$	=	upstream stagnation pressure
q	=	up stream dynamic pressure ($\rho U^2_\infty /2$), ρ = upstream density
Re	=	Reynolds number based on the chord length of the airfoil ($\rho U_\infty c / \mu$)
α	=	angle of attack
L/D	=	lift to drag ratio or glide ratio
δ_1	=	displacement thickness
δ_2	=	momentum thickness
U	=	local free stream velocity outside boundary layer
U_∞	=	upstream velocity
u	=	fluid velocity in the stream wise direction

* President, Sinhatech, and Senior Member AIAA

v = fluid velocity normal to the stream wise direction
x = distance from the leading edge along chord or streamwise coordinate for flow equations
y = wall normal coordinate for flow equations
τ_w = wall shear stress

I. Introduction

Increasing the extent of laminar flow is deemed desirable for high performance wings. As a result, high-performance sailplanes representing the pinnacle of aerodynamic efficiency have fine tuned wing profiles to maintain laminar flow over the entire lower surface and from the leading edge to about 85-90% of the chord on the upper surface. This has culminated in modern 15-m wingspan standard-class sailplanes (without flaps) attaining a best glide ratio (L/D) of 48-50 with a wing aspect ratio around 22[1]. A sailplane with an aspect ratio 51.3 wing with flaps similarly optimized for extensive laminar flow has attained a best L/D of about 70[1,2]. This is believed to be close to the performance limit, since increase in parasitic drag C_{do} overcomes reduction in induced drag C_{di} if the wing aspect ratio A_r is increased. Maximizing laminar flow has also been followed by long-endurance unmanned aerial vehicles, where maximizing $C_L^{3/2}/C_d$ is desired. However, the airspeed for best endurance occurs at a higher C_L than the point at which L/D maximizes. This brings it closer to stall and the UAV designer typically has to settle for a lesser extent of laminar flow on the wing upper surface to prevent flow separation. Additionally, laminar flow requires maintaining extremely smooth surfaces which is practically impossible for commercial and general aviation aircraft under actual operational conditions. Therefore, airfoil designs for such aircraft tend to somewhat conservative and also settle for a lower L/D. For example, the philosophy embraced by NASA in their NLF series General Aviation airfoils required the performance to be no worse than comparable turbulent profiles even when contaminated by surface roughness and leading-edge bug hits. Airfoils for wind-turbine blades have even more stringent requirements since they operate in a high-debris environment close to the ground. While applying active

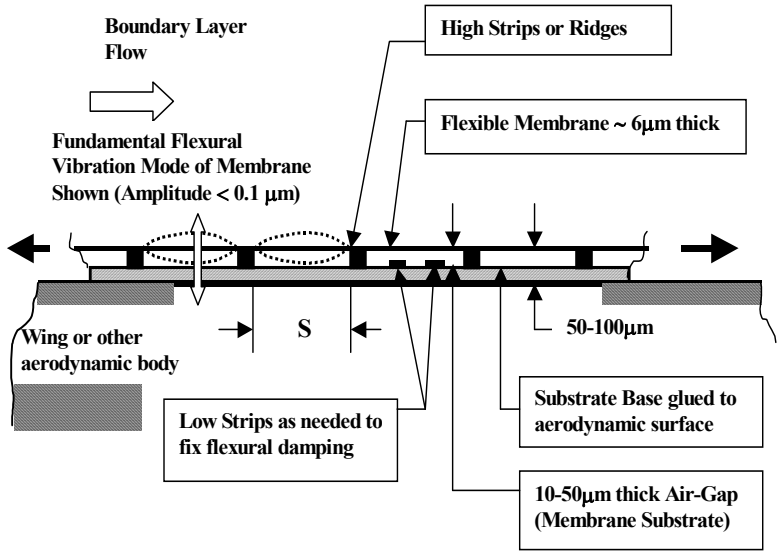

Fig 1. Schematic of the SINHA Flexible Composite Surface Deturbulator (FCSD)

flow control can extend laminar flow, the performance levels will not significantly exceed current generation sailplanes. The reason for striving towards perfect laminar flow is the lower skin friction attributed to laminar versus turbulent boundary layers under otherwise identical conditions. An attached laminar boundary layer still has non-zero skin friction, while a separated boundary layer has zero or slightly negative skin friction. It would appear that separation followed by reattachment, such as in a laminar separation bubble, offers the lowest drag solution. However, this is not so because of higher rates of thickening of the adverse pressure gradient boundary layer following laminar-turbulent transition of the separated shear layer. One way of minimizing rapid thickening of adverse pressure gradient boundary layers is to shape the wall such that the pressure gradient maintains the boundary layer on the verge of separation[3]. This also allows greater suction on the top surface, thereby increasing C_L. The other approach is to devise a method for attenuating turbulent mixing in the separated shear layer and is the focus of the current paper.

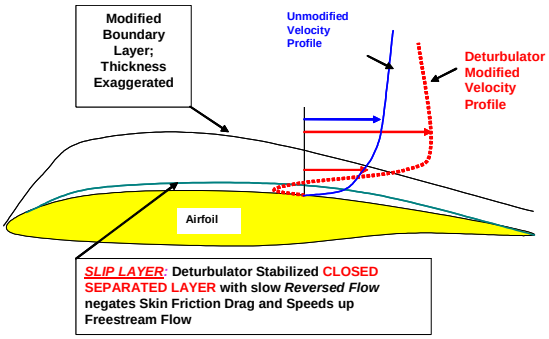

Fig 2. Separated "Slip Layer" eliminates skin-friction drag. Adverse pressure gradient drives reversed flow. The FCSD attenuates mixing across the Slip-Layer and prevents it from breaking down.

Earlier studies by the present author with his Flexible-Composite-Surface-Deturbulator or FCSD[4-8] (Fig 1) proved the method works. Even though the Deturbulator (Fig 1) appears to be a manifestation of a "compliant wall", it is significantly different. Earlier compliant walls were aimed at damping instabilities in attached laminar boundary layers to delay transition or counteracting wall-normal velocity components in turbulent boundary layers[9-11]. The precise matching of fluid and wall motion needed for this form of control has only been realized in experiments where controlled disturbances were introduced and subsequently annulled by the wall motion. Hence earlier experiments involving compliant or externally actuated flexible walls on attached and usually zero-pressure-gradient boundary layers have however failed to show appreciable repeatable drag reduction in real flows[9]. Additionally, devising compliant walls for low-speed air flows has been considered impractical due to material property constraints[11]. The FCSD has overcome these constraints and succeeded since it relies on using a localized flow-device interaction to modify a non-zero pressure gradient flow with regions of marginal boundary layer separation. It also does not rely on damping within its structure to attenuate turbulent fluctuations.

The FCSD or "Deturbulator" provides a way of modifying the turbulence spectrum by directly breaking down the larger turbulent eddies into smaller ones. This bypasses the normal turbulent cascade and can be used to attenuate turbulent mixing in regions of high shear. This stabilizes separated shear layers and enables thin and long non-dissipative closed separated regions over a significant extent of the chord (Fig 2). The separated region behaves as a "slip layer" by negating skin-friction and also provides a more cambered virtual shape to the wing profile as seen by the inviscid outer flow. As a result the section lift coefficient is also increased. This paper examines the limits of L/D enhancements using the Deturbulator in view of recent in-flight verification of this method.

The Technology and Device: The SINHA-FCSD[4-8] is a thin (under 100 μm) passive (i.e., non-powered) device (Fig 1), consisting of a flexible membrane (typically 30-300 mm wide) stretched across an array of strips on a substrate, running in the spanwise direction. The back of the substrate is bonded to the surfaces of the wing or stabilizer, typically near the aft section of the airfoil for advanced low-drag wings, where marginal separation of the attached aerodynamic boundary layer leads to large increases in drag especially for high wing loadings. Under design conditions, the membrane of the FCSD undergoes extremely small (under 0.1-μm amplitude) flow-induced flexural oscillations, which can neutralize turbulent fluctuations in the near-wall slightly separated boundary layer airflow (Fig 2a). The resulting modified boundary layer, which has an imbedded "slip layer" displays superior resistance to separation as compared to a laminar boundary layer (i.e., reduced δ_1, δ_2)[5,6] while exhibiting lower skin-friction induced losses compared to either "naturally occurring" or artificially tripped turbulent boundary layers. This results in a reduction in wing profile drag. The current passive SINHA-FCSD concept evolved out of an earlier electrically powered Active Flexible Wall (AFW) boundary layer control concept[12-14] which has undergone extensive low-speed ($M < 0.15$) wind tunnel testing at the University of Mississippi primarily for controlling unsteady flow separation[13,15]. Unlike earlier compliant and driven flexible wall devices which were typically tested on flat-plate zero pressure gradient flow[9], the AFW and FCSD have been found to work only in boundary flows exposed to a varying streamwise pressure gradient. To understand the flow-membrane interaction mechanism the 2-D streamwise u-momentum equation[16] of the flow at the mean equilibrium position (y = 0) of the surface membrane of the FCSD is considered first:

$$v(\partial u/\partial y)_{y=0} = -(1/\rho)(\partial p/\partial x) + (\mu/\rho)(\partial^2 u/\partial y^2)_{y=0} \qquad (1)$$

The streamwise x-component of velocity "u" of the vibrating membrane (or the velocity of the fluid at the points of contact with the membrane) has been assumed to be negligible, while the wall-normal y-component of velocity "v" of the fluid next to the membrane is clearly non-zero due to membrane compliance. Key to flow-membrane

interaction is the realization that the wall-normal gradient of the streamwise velocity at the wall, $(\partial u/\partial y)_{y=0}$, can be extremely large at certain x-locations. At such locations, even a small oscillation velocity ($v << U$) of the flexible membrane can make the $v(\partial u/\partial y)_{y=0}$ "control" term on the left hand side of equation (1) predominant enabling dynamic coupling of turbulent velocity fluctuations in the freestream with the FCSD. For a non-porous, non-compliant wall, this control term is identically zero. Additionally, if the boundary layer velocity profile at the aforementioned locations is such that prior to interaction $\partial^2 u/\partial y^2_{y=0} \approx 0$, while $|(\partial u/\partial y)_{y=0}| > 0$, (i.e., u(y) is approximately linear near the wall) an order of magnitude balance of the terms in equation (1) yields:

$$v(\partial u/\partial y)_{y=0} \approx -(1/\rho)(\partial p/\partial x) \qquad \textbf{(1-a)}$$

Such a condition can be satisfied in boundary layers over curved surfaces, in the vicinity of x-locations where the streamwise pressure gradient $\partial p/\partial x$ changes from favorable ($\partial p/\partial x < 0$) to adverse ($\partial p/\partial x > 0$). The FCSD also passes oscillations with minimum damping at the control frequency[4-8]:

$$f = U/s \qquad \textbf{(1-b)}$$

Fig 3 shows how large scale vortices, imparting long-wavelength traveling waves on the membrane of the Deturbulator, are broken down to smaller vortices of wavelength "s" corresponding to the frequency f. Since f is closer to the "dissipation range" the smaller vortices are quickly smeared out by molecular viscosity and a large section of the normal step by step process of eddy breakdown[17] through vortex stretching and bending is avoided. This attenuates turbulent mixing and entrainment across regions of sharp velocity gradients and helps stabilize the marginally separated boundary layer with its inflectional velocity profile as shown in Fig 2. The stabilized and nearly stagnant separated region acts as a slip-layer by keeping the fast moving outer flow off the wall. Fig 7b shows an oil flow visualization of this layer.

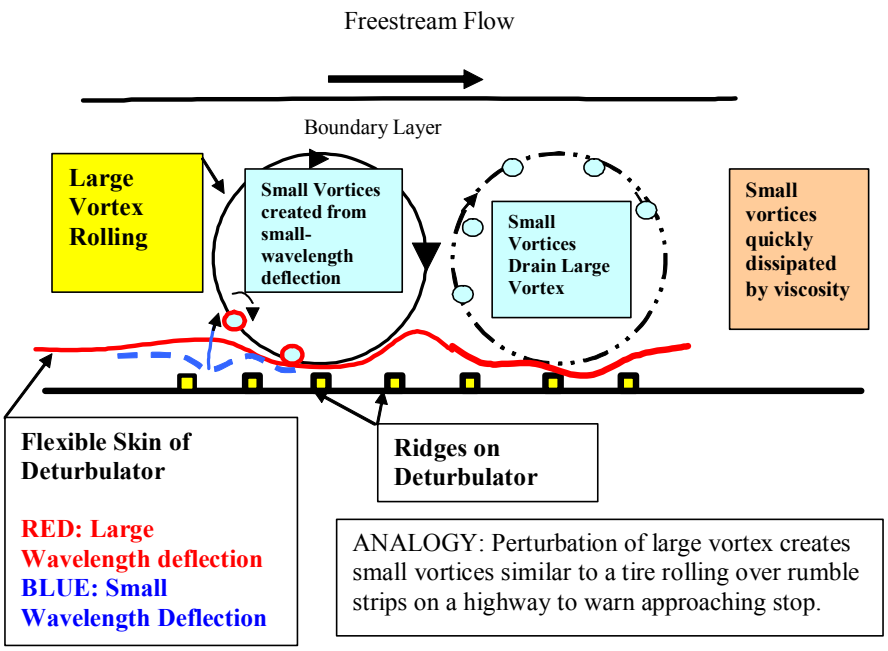

Fig 3. Sketch illustrating how the Deturbulator breaks up large vortices

The action of the Deturbulator is similar to vibrations transmitted to an automobile tire rolling over "rumble strips" warning an on oncoming stop sign. This slows down rapid mixing in regions of high shear[16-17]. Since the separated shear layer is prevented from thickening through turbulent mixing, increased form drag typical in separated zones is avoided. The skin-friction can be zero or negative over extended lengths, which is not attainable by maximizing attached laminar flow.

The Deturbulator can also reduce turbulence in larger separated regions, such as in bluff-body wakes. The quiescent separated wake behaves as a virtual streamlining extension and reduces form drag[18].

For the dynamic interaction depicted in Fig 3 to exist and maximize as per equation (1-b), the Deturbulator tape needs to be located only within a certain receptive zone. This requires knowledge of the viscid and inviscid flow over the base airfoil and can be expected to vary with airfoil profile, Re, M, α and surface roughness. Additionally, the thickness of the Deturbulator tape itself modifies the airfoil profile and this effect can be utilized to encourage the boundary layer to undergo marginal separation as shown in Fig 4. If optimally done, the boundary layer on the surface of the Deturbulator remains attached while marginal separation extends both upstream to the leading edge and downstream to the trailing edge. On the upper surface of a wing depicted in Fig 4, this speeds up the inviscid freestream and increases the circulation, effective camber and section C_L. The Deturbulator tape needs to be wide enough to cover the excursion of the receptive zone across the desired range of airspeeds and wing loading. Additionally, the ridge spacing of the Deturbulator needs to be tailored such that the frequency f is close to the dissipation range of the turbulence for the range of freestream velocities.

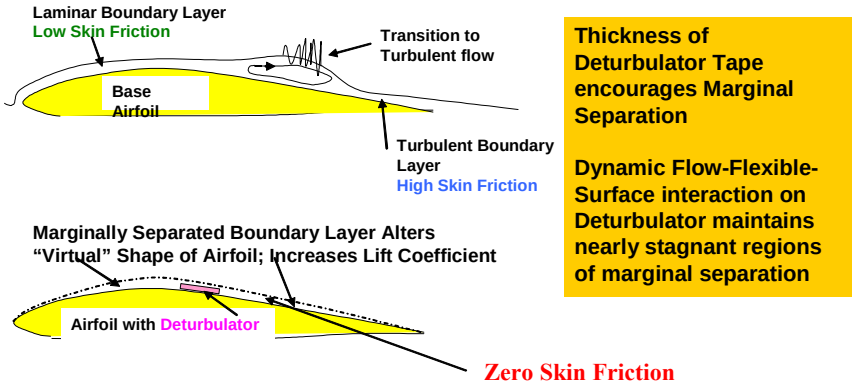

Fig 4. How the Deturbulator encourages boundary layer separation and stabilizes the slip layer to virtually morph the camber of the airfoil while eliminating skin friction

II. Technical Approach

Details of the aforementioned phenomenological explanation are extremely difficult to observe due to sub-micron scales involved normal to the wall, along with scales about 5-orders of magnitude larger along the flow. These have to be indirectly inferred from larger scale measurements which do not upset the process. Much of the reasoning, such as the control frequency f and flow flexible-wall interaction physics is based on earlier wind-tunnel tests with the AFW[12-14]. Hence, a decision was made to proceed with flight tests to establish the overall validity of the FCSD system as opposed to resolving small-scale details of the constituent process first.

Early tests of FCSD patches on a NLF-0414F wing of a GT-3 all-composite trainer aircraft (manufactured by Global Aircraft, Starkville, MS) indicated 17-27% boundary layer momentum recovery on the top and bottom surfaces as measured in flight at Re ≈ 5-million[4]. Subsequent tests on the same wing showed profile drag reductions in the range of 12-25% at Re ≈ 4 to 6-million as measured with trailing edge mounted drag rakes[5]. Low-speed wind tunnel tests at Re = 0.3-million on the NLF-0414F airfoil showed the FCSD capable of reducing profile drag and enhancing lift in spite of separated flow near the trailing edge, resulting in a 12% enhancement in section L/D. In all these tests the Mach numbers remained below 0.16.

Tests on the Standard Cirrus sailplane (manufactured in 1970 by Schemp Hirth, Germany; shown in Fig 5) facilitated the optimum location of the Deturbulator tape since the wing root section airfoils, transitioning linearly from the Wortmann FX S 02-196 at the root to the Wortmann FX 66-17 A II-182 at the inner end of the aileron are capable of operating over a wider range of Reynolds numbers (0.2-4 million) without undergoing breakaway boundary layer separation. Also, the pressure distributions over these airfoils do not change drastically within this Re range even though laminar flow is maintained over about 30% of the top surface. Thus, low-speed wind tunnel results can be more readily extrapolated to flight conditions. Earlier papers by Sinha and Ravande[5,6] describe test results, beginning with low-Re wind-tunnel tests of wing airfoil sections and culminating in treating the entire span

of the wing to achieve 18% reported increase in best L/D based on independent in-flight sink rate measurements by Johnson[19]. The focus of this work is on observable effects guiding the optimization procedure for installing the Deturbulator on the Standard Cirrus wing. These results are part of an ongoing developmental process aimed at increasing L/D and $C_L^{3/2}/C_d$.

.

Fig 5. The Standard Cirrus, 15-m wingspan, single seat, all composite test sailplane

Initial flight tests[6] were conducted with a 600-mm long FCSD strip mounted on the lower surface of the wing of the Standard Cirrus. The strip was centered on the inboard section of the 15-m span wing, 1.32-m (53 inches) from the wing-fuselage joint. The 813-mm chord wing section at this spanwise location is a linear transition from the Wortmann FX S 02-196 at the root joint to the Wortmann FX 66-17 A II-182 at a spanwise location of 4.17-m outboard (beginning of ailerons). A wing-trailing edge mounted drag probe (rake) incorporating an array of total head tubes connected to a common header and encompassing 12.5-mm (1/2") of the wing top and bottom boundary layer at the trailing edge, was used to monitor changes in the wing wake. The top holes of the probe were taped off for bottom surface measurements and vice versa. A calibrated temperature compensated differential electronic pressure transducer was used to measure the difference between the stagnation pressure from the aircraft's pitot-static probe and the integrated drag-probe stagnation pressure. The pressure transducer output (Volts) gives a direct indication of the profile drag from the wing bottom or top. A reduction in Voltage output indicated drag reduction on the lower surface. However, a lower surface Deturbulator also reduces positive camber and reduces section C_L.

Early tests on the upper surface at the 52-53 inch span station did not result in drag reduction. This prompted the wind tunnel studies described below.

Wind Tunnel Setup

The SINHATECH low-speed Wind Tunnel used in these tests has an entrance 4-ft high and 3-ft wide with an exponential contraction down to the 12-inch high, 9-inch wide test section. 127-mm chord, 190-mm span stereolithographed hand-smoothened and painted models of the 53-inch (1.346 m) span airfoil and tip airfoil (Wortmann FX 66-17 A II-182 outwards from 4.17-m span) of the Standard Cirrus wing section were tested. Various locations of the Deturbulator were screened using a 1-chord height wake rake placed ½-chord behind the trailing edge. Tests were run at Re = 300k and M = 0.09 over a range of α values (Fig 16).

Deturbulator Tape and Installation:

Test Deturbulator tapes for the wind-tunnel and flight tests were fabricated by SINHATECH using in-house prototyping facilities. The ridges (Fig 1) were 2-mm apart with a single row of low strips 15-μm lower in between the high strips. These dimensions provide f ~ 7.5 kHz to 25 kHz for airspeeds between 15-50 m/s. A 6-μm thick aluminized Mylar sheet, whose edges were either taped to the airfoil surface, or in the final design glued to the edges of the substrate, was used as the flexible membrane. The overall thickness of the FCSD tape was about 80-μm. The substrates had pressure sensitive adhesive backing and had widths varying from about 6-mm to 50-mm and lengths from 150-mm to 500-mm depending on application . The FCSD strips were oriented with the ridges on the substrate running spanwise. Also, the cavity between the membrane and substrate (Fig 1) was vented to the freestream such that reduction in ambient pressure due to altitude and increased airspeeds did not lift the membrane off the ridges.

Flight Performance Tests:
These involve towing the sailplane to an altitude above thermal activity and maintaining constant indicated airspeeds during subsequent descent, while recording altitude. The rate of descent gives the sink rate from which L/D can be estimated. Since vertical air mass movements can bias readings, an average of several readings is needed. Alternately, the test sailplane can be flown in parallel against another calibrated sailplane within the same air mass. Details of conducting tests, including instrument calibration are described in Johnson's article[19].

III. Results

Wind tunnel tests on the 5-inch (127 mm) chord Standard Cirrus 53-inch span-section airfoil model were conducted at Re = 0.3 million and M = 0.1 with and without FCSD strips[5,6]. Surface oil flow patterns of the clean wing at an angle of attack $\alpha = -1°$ indicated a separation bubble on both top and bottom surfaces (as the region where the oil accumulated). Even though the surface of the model had been slightly over-sanded, the positions of the separation bubble matched closely with those indicated in the surface pressure distribution plot in an XFOIL[20] simulation for this airfoil under identical conditions shown in Fig 6. The separation bubbles are seen as bulges in the C_p versus x/c plot of Fig 6. A variety of suction side FCSD treatments were screened for this airfoil model using the drag-rake measurements for α values ranging from $-2°$ to $+2°$ in steps of 1° (Fig 16). In all FCSD cases a nominal 6-mm (0.25-inch) wide substrate was employed with the Mylar membrane taped to the airfoil surface with 32±1 μm thick Tesa tape (normally used for taping over wing-fuselage joints in sailplanes). The location was based on applying the criterion of Equation (1a) as far as possible with adjustment for flow features unique to this situation.

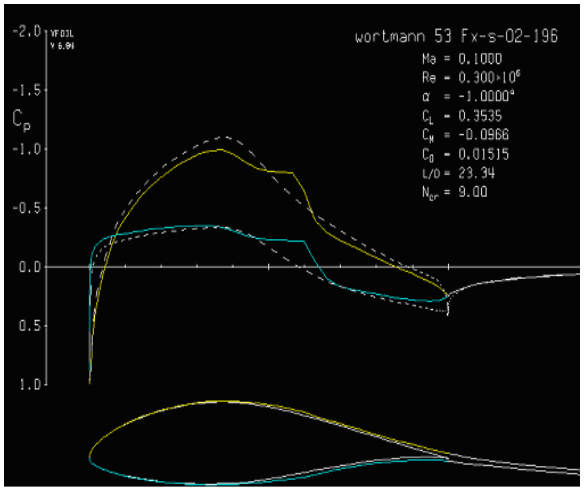

Fig.6. XFOIL Simulation of Flow on 5-inch Chord Wind Tunnel Model of Std. Cirrus 53-inch Span Airfoil Section showing C_p Distribution on Suction (yellow) and Pressure (blue) Surfaces at $\alpha = -1°$, Re = 0.3 million and M = 0.1

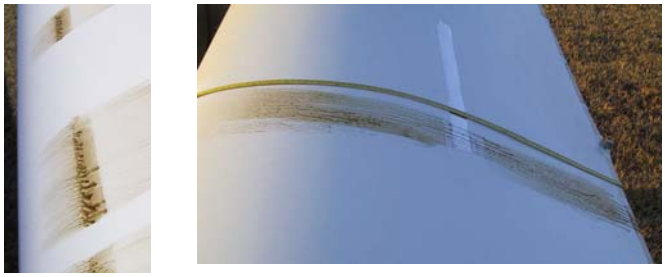

a b

Fig 7. Oil Flow Visualization on Top Surface of the Standard Cirrus wing at the 53-inch Span Station (a) untreated; (b) with Deturbulator shown.

Fig 7 shows oil flow visualizations on top of the wing with and without Deturbulator treatments at an indicated airspeed of 70-kt. This corresponds approximately to **$\alpha = -1°$, Re = 1.5 million and M = 0.11.** The same x/c location of the center of the Deturbulator strip was used was used for these flight tests as well. The untreated wing has a strong laminar separation bubble on the upper surface seen from the accumulated oil in Fig 7a, which ends in turbulent breakdown. The Deturbulator appears to remove the bubble similar to a turbulator or vortex generator. However, a closer examination of Fig 7b shows that the separated zone has not been removed, but

extended from slightly behind the leading edge to the trailing edge as evidenced from the visibly stagnant oil layer (i.e., the slip layer). No turbulent breakdown resulting in rapid thickening of the oil is visible.

Fig 8. Clean wing 30º bank (top) versus 60% inboard span FCSD treated 45º bank (bottom). Lower wing deflection even under higher loading (bottom) is due to increased lift from inboard sections.

Fig 8 shows in-flight photographs of the wing with the center 60% of the span treated with the Deturbulator. Even with a higher wing loading resulting from a steeper bank (45º versus 30º), the Deturbulated wing does not bend as much. This is a visible confirmation of increase in C_L of the Deturbulator treated center section, since this unloads the tip sections and reduces the bending moment.

Fig 9 shows a full-span Deturbulator installation on the Standard Cirrus as tested by Johnson[19] while Figs 10 and 11 show his sink rate and L/D polars based on sink rate measurements from three Deturbulated and three clean-wing flights.

The 48-kt calibrated airspeed point shows a persistent 18% improvement in L/D that is well above the 4th order polynomial fit through the data points.

Fig 9. Full-Span upper surface Deturbulator on Std. Cirrus as evaluated by Johnson[19]. (50-mm wide Deturbulator Tape with Vents between 200-300 mm long segments)

The minimum sink rate (at 37-kts) is 3.5% lower and remains almost unchanged till the point of maximum L/D.

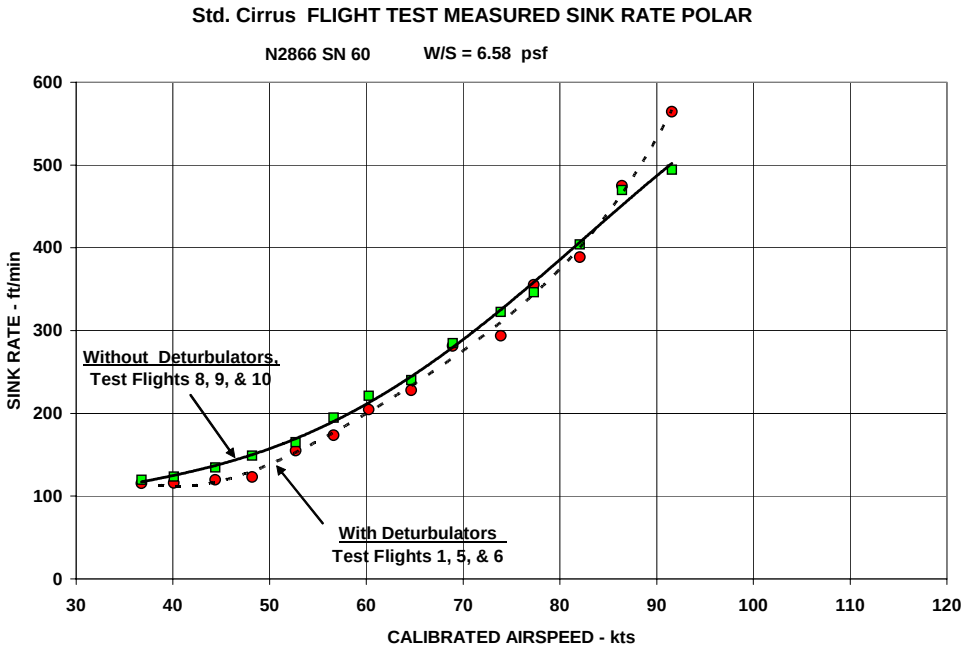

Fig 10. Measured Sink-Rates for Standard Cirrus with 4th order fit trend lines (Johnson[19])

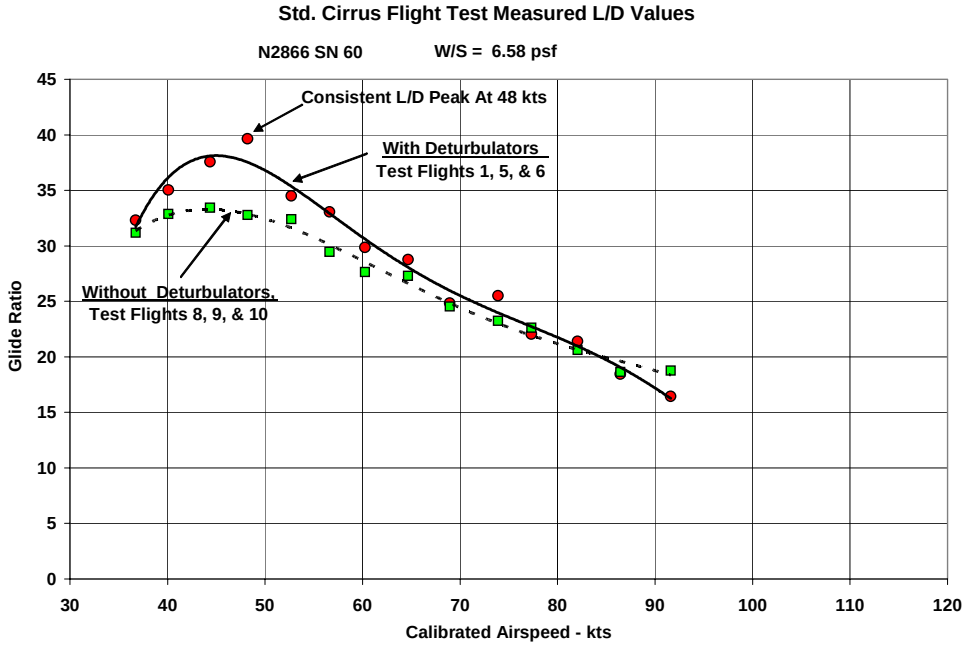

Fig 11. Measured L/D for Standard Cirrus with 4th order fit trend lines (Johnson[19])

The best L/D of 39.7 occurs at 48 kts as opposed to a best L/D of 33.4 at 44 kts calibrated airspeed. Fig 12 shows a plot of C_d versus C_L^2 with straight lines of the form $C_d = a.\ C_L^2 + C_{do}$ fitted to the baseline and Deturbulated data points. The slope of the line is $a = (k + 1/(e\pi A_r))$, where $k\ C_L^2$ represents a parasitic drag term (i.e., does not contribute towards the vortex system needed to generate lift). This adds on to the constant term C_{do} representing parasitic drag at zero lift. Under ideal conditions with perfect elliptical distribution of lift across the span (i.e., k = 0 and e =1), the slope "a" of the C_d versus C_L^2 line is $1/(\pi A_r) = 0.0145$, which is lower than either the baseline or Deturbulator treated values in Fig 12. If the full span Deturbulator maintains this ideal distribution, the total sailplane drag coefficient at the 48-kt (best L/D) point should be:

$$\mathbf{C_d = C_{do} + C_{di} = 0.0128 + 0.0145\ C_L^2 = 0.0228} \quad \mathbf{(2\text{-}a)}$$

In contrast the measured C_d at this point is 0.0210. This is lower, signifying a 8% reduction in total parasitic drag. Since the value of Oswald's span efficiency factor e is most likely less than unity, the actual reduction in parasitic drag is greater. If the aforementioned analysis is repeated for the adjacent 44-kts and 52-kts points, which fall more closely on the trendlines in Figs 11 and 12, a 2.6% reduction and 1.9% increase in parasitic drag are shown respectively. The untreated best L/D point (at 44-kts) also shows 7.8% higher parasitic drag compared to the predicted C_d value for the untreated wing with a perfect elliptical span loading. The predicted value is:

$$\mathbf{C_d = C_{do} + C_{di} = 0.0133 + 0.0145\ C_L^2 = 0.0273} \quad \mathbf{(2\text{-}b)}$$

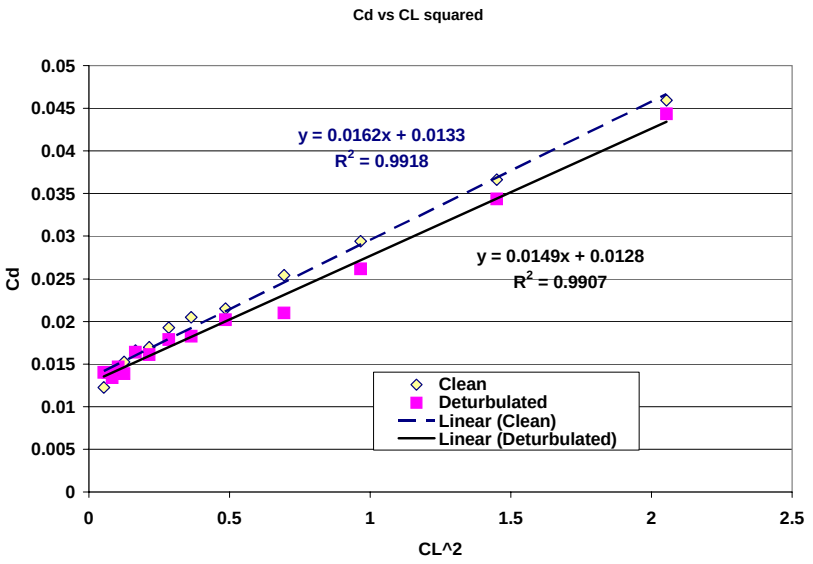

Fig 12. A plot of C_d versus C_L^2 for the Standard Cirrus based on the data of Fig 10 and Fig 11. The equations of the best fit straight lines are also shown along with values of the correlation coefficient R.

IV. Analysis and Discussions

The aforementioned analysis reveals a large reduction in parasitic drag (more than 8%) at the best L/D point when the Deturbulator is installed. ***Is this the maximum that can be achieved for the Standard Cirrus? Was the Deturbulator working optimally?***

To answer these questions all the data need to be examined to see if the discarded data in Johnson's Flights 2, 3 and 4 with the Deturbulator reveal trends. After determining the L/D and sink-rate polars using data from all flights Johnson[19] discarded the data from these flights assuming the rather large variations were due to vertical air movement. In Figs 13-15, measured L/D and sink rates are plotted based on the day the data was obtained. On Day-1, Deturbulated-wing Flights 1-4 were executed with very little time between flights. The same was done for Flights 5 and 6 on Day-2. Each flight started with a tow to 13-k ft altitude during which time the ambient temperature and

pressure dropped. The vents in between Deturbulator tape segments (Fig 9) were designed to equalize pressures during ascent and descent. Johnson[19] concluded that airflow between the ridges of the substrate were not fast enough to do this effectively. The test data showed temperatures above about 3000 ft altitudes dropped below the dew point temperature of the ground level air. Hence moisture condensed in the air trapped in the Deturbulator cavity. Liquid water has been known to force the Mylar membrane to stick to the substrate on the type of Deturbulator used, impeding venting and membrane oscillations (www.sinhatech.com). Increasing ambient pressure during unabated descent during most of the test flights (Figs 13 and 14) exasperated sticking down of the membrane. However, during the subsequent slow ascent during tow, reduction in ambient pressure probably forced out some of this moisture through the vents. Repeating this process makes more of the Deturbulator operational. This trend is clearly seen on days 1 and 2. L/D increases as sink-rates fall with each subsequent flight. At low speeds, dramatic improvements in L/D and sink rate are observed between Flights 1 and 4 in Figs 13. Fig 14 also shows lower sink rates for Flight 6 versus Flight 5. In contrast this is not seen in the tree flights on Day-3 (Fig 14) with Deturbulator removed. Also, the (75-100 ft/min) variations in sink rates at 48-kts is two-three times as high with the Deturbulator even when compared to the maximum variations with clean wing (29 ft/min) at the lowest speed. Historically, published flight test data obtained by Johnson show 30 ft/min maximum variations in measured sink rate, with an average variation of 21 ft/min (www.sinhatech.com). Hence it is very likely that the large excursions in Figs 13 and 14 are due to inconsistencies in Deturbulator behavior and not due to air movement.

Fig 16 shows wind tunnel wake-drag-rake data used for optimizing the location of the Deturbulator on the chord of the 53-inch span Standard Cirrus airfoil model. The last two configurations in Fig 16 are identical except for heat shrinking the Mylar membrane immediately prior to testing in the final case. Heating also removed residual moisture and greatly improved the drag reduction. This not only shows the detrimental effect of moisture with a loose membrane but also suggests greatly improved L/D if such problems are mitigated on the prototype wing. This may have occurred for example, during Flight 4 (Fig 13), which shows an L/D of 68 at 48 kts. However, is this feasible?

The best L/D ratio for an aircraft can be estimated by assuming this occurs at an airspeed at which the total drag is minimized in steady non-accelerated flight[21].

$$\mathbf{(L/D)_{max} = [\pi e A_r (A/A_w)/(4C_f)]^{1/2}} \qquad \mathbf{(3\text{-}a)}$$

For the untreated Standard Cirrus, $e \approx 1$, $A_r = 22$, $A/A_w \approx 0.4$. This yields $C_f = 0.0062$ for $(L/D)_{max} = 33.4$. If the Deturbulator simply eliminates skin friction from the upper surface of the wing, the ratio of total wetted area to the wing planform area, A/A_w increases to 0.635. With the same value of C_f, we obtain $(L/D)_{max} = 43$, which is close to the average 48-kt value in Fig 11. For $(L/D)_{max} = 65$, we need C_f to reduce to 0.0025. This can happen if the morphing of the airfoil due to the Deturbulator reduces pressure drag as well by making the higher virtual cambered wing operate at a lower angle of attack. The Deturbulated Standard Cirrus has been found to operate at a more nose-down attitude. Pressure drag increases at slow airspeeds and high α, when the wing lift-slope ($dC_L/d\alpha$) begins to drop from its linear value. Increasing the camber of the wing section airfoils reduces the zero-lift angle of attack, generating the same C_L at a lower α, within the linear portion of the lift-slope curve. This lowers separation induced pressure drag at low speeds. Additionally, any separated zone can be made more stagnant by the Deturbulator[12], reducing pressure drag even more.

An alternate representation of $(L/D)_{max}$ can be found from equations 2-a or 2-b (i.e., $C_d = a.C_L^2 + C_{do}$), as:

$$\mathbf{(L/D)_{max} = 1/[4a.C_{do}]^{1/2}} \qquad \mathbf{(3\text{-}b)}$$

For the clean wing, using values of a and C_{do} from equation (2-a), $(L/D)_{max} = 34.0$. This is very close to the measured value of 33.4. For the Deturbulated wing, using values of a and C_{do} from equation (2-b), $(L/D)_{max} = 36.2$, This is significantly lower than the best L/D = 39.7 at 48-kts. If the upper surface of the wing does not generate skin friction or pressure drag, the value of C_{do} is approximately halved. This increases $(L/D)_{max}$ to 52, which is slightly higher than the best for 15-m standard class sailplanes with maximum laminar flow. The nose-down attitude from increased virtual camber from the Deturbulator can further improve upon this value by helping reduce the total parasitic drag of the wing. This can be visualized as reducing the effective wetted area of the sailplane. If 85% of the wing surface is made drag free, $(L/D)_{max} = 65$ as per equation (3-a). The best optimized Deturbulator treated 53-inch span section test data of Fig 16 suggests that this is possible.

Improvements in Deturbulator materials and design are currently underway to address problems with moisture accumulation and venting. An improved design with hydrophobic coatings and vent inserts has performed well on automobiles and trucks under a variety of weather conditions, including rain[18].

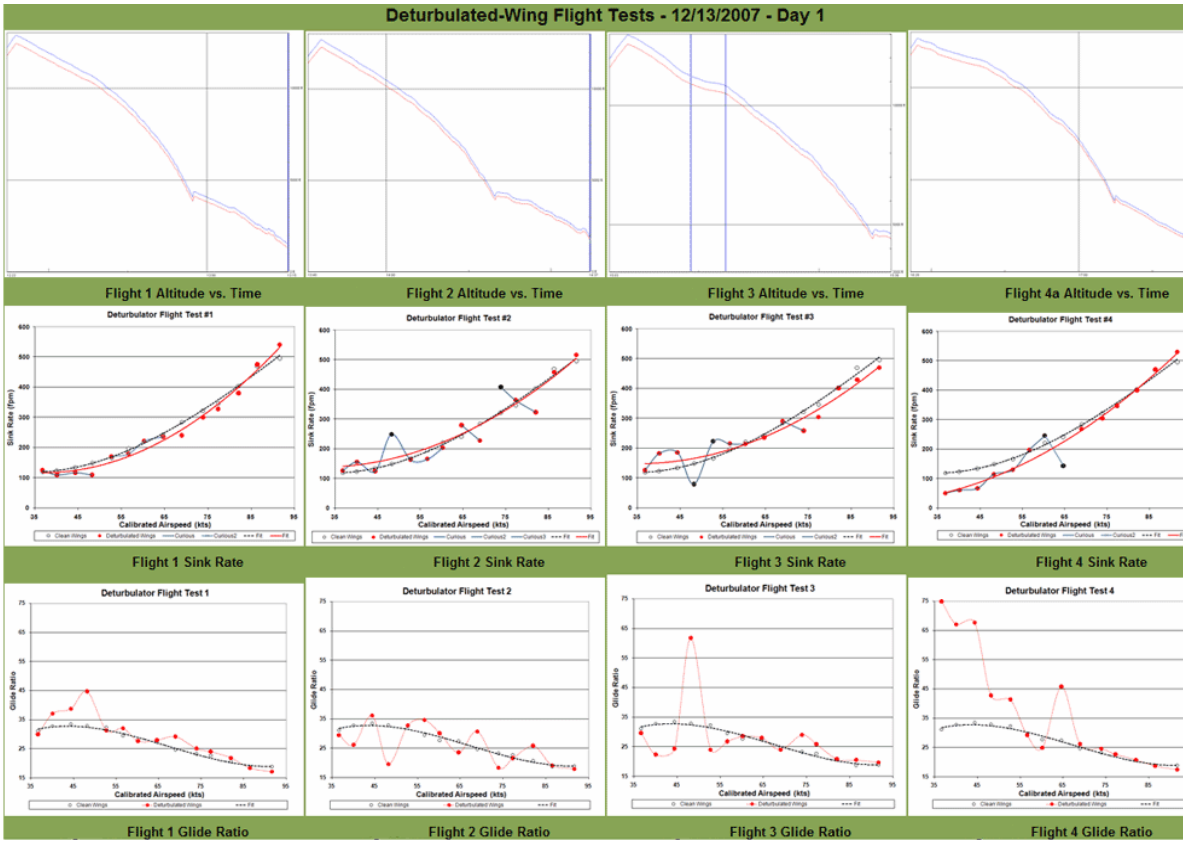

Fig 13. Altitude versus time (top row, blue-geometrical GPS altitude, red-pressure altitude), Sink rates (mid row) and L/D (last row) for Johnson's Flights 1-4 (left to right) on Day 1, with the Deturbulated Standard Cirrus (Red) versul clean wing (black). Note flattening out of low speed glide slope with progressive flights. Lines joining data points are simply to aid visualization and do not represent trends

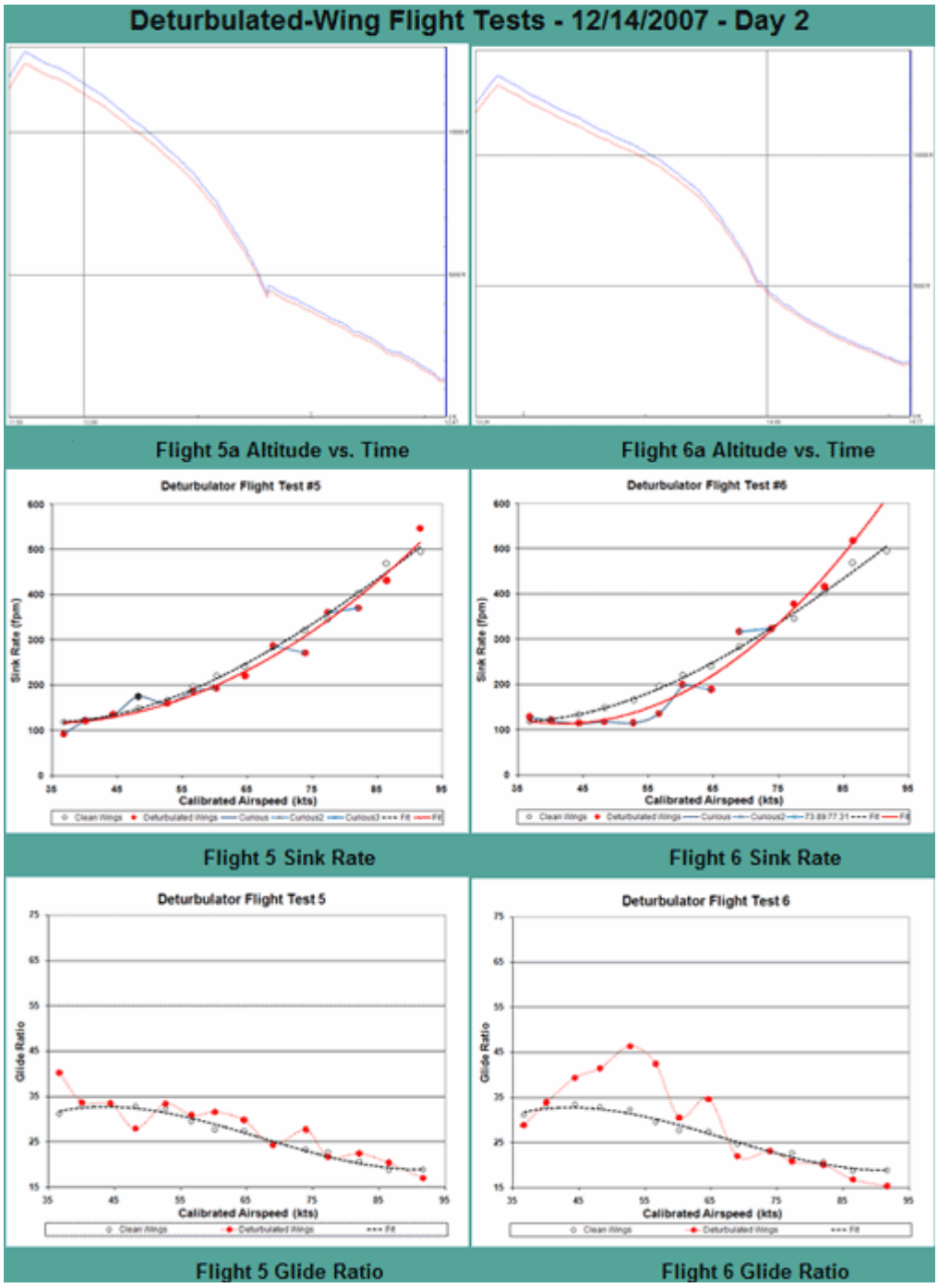

Fig 14. Altitude versus time (top row), Sink rates (mid row) and L/D (last row) for Johnson's Flights 5 and 6 4 (left to right) on Day 2, with the Deturbulated Standard Cirrus. (see notes on Fig 13).

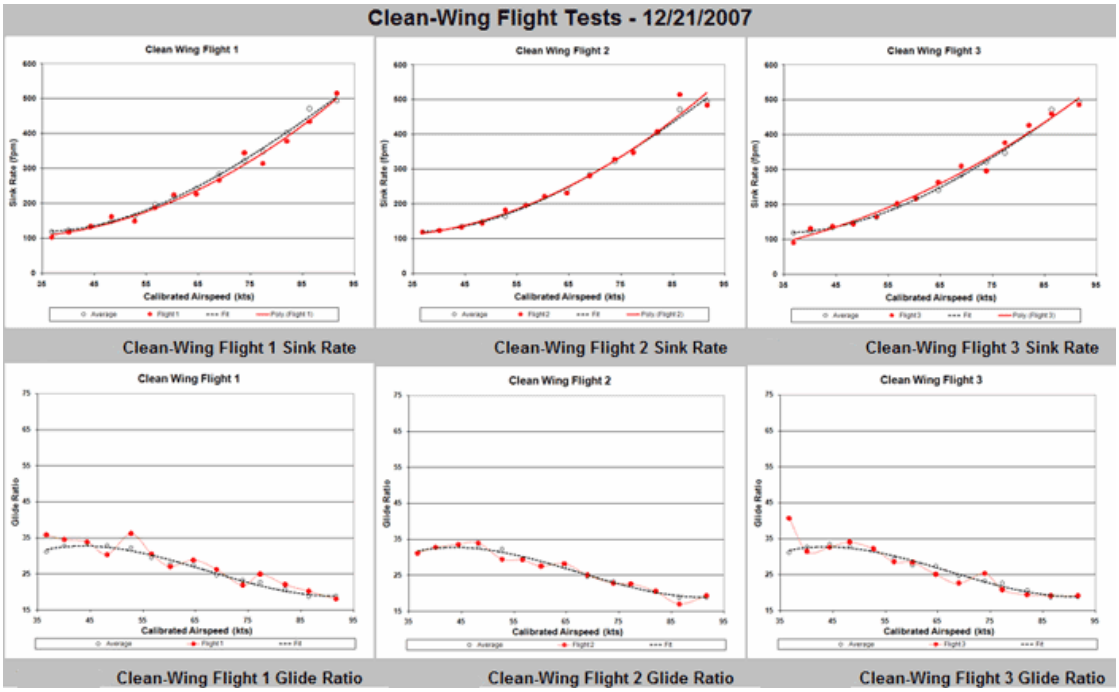

Fig 15. Sink rates (top row) and L/D (last row) for Johnson's Flights 7 -9 (left to right) on Day 3 ,for Standard Cirrus with Deturbulators removed.

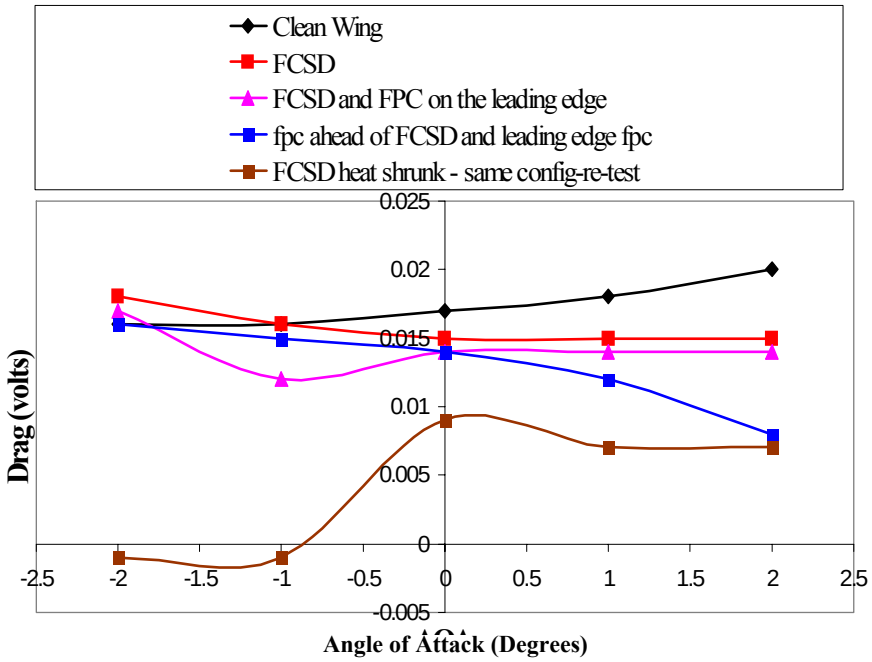

Fig16. Optimization of Deturbulator (FCSD) installation on wind-tunnel model of Standard Cirrus 53-inch wing span station airfoil. Wake Drag Rake pressure sensor output (volts, proportional to section C_d) versus angle of attack. (Note: Data not corrected for wind tunnel blockage)

V. Conclusions

A passive flexible wall flow control device, the Deturbulator has been developed that can be affixed to selected x/c locations on an aircraft wing surface to permit the boundary layer to separate but not break down through turbulent mixing. The Deturbulator converts large-scale turbulence producing vortices to smaller eddies, at a single high frequency. The smaller eddies which are quickly dissipated. This bypasses the normal turbulence cascade.

The flow in the separated region is made nearly stagnant if the dynamic coupling is maximized between the flexible wall with fluctuations across the boundary layer at a point where the streamwise pressure gradient is close to zero.

Multiple in flight sink-rate measurements of a Standard Cirrus sailplane verified an 18% increase in average best glide ratio (L/D) by treating about 8% of the mean aerodynamic chord of the wing upper surface, across the entire span with Deturbulator tape. The data displays a 93% confidence that L/D increased by at least 5 counts to 38. This however was not an entirely optimum situation since flight-to-flight variations in sink rate were three to four times the non-deturbulated values. Variations in non-deturbulated wing sink rates were consistent with historical variations in similar tests on a variety of sailplanes. The variations appear to be a result of degradation in Deturbulator performance due to combined temperature, pressure and humidity changes during ascent followed by descent in each flight.

If the Deturbulator operates optimally, 100% enhancement in best L/D is revealed from selected measured sink rate data. Wind-tunnel data from optimized Deturbulator installation on the wing airfoil model shows such increases possible. An analysis using simplified flight performance equations indicate reducing 85% of combined pressure drag and skin friction of the wing is needed to achieve this.

An optimized Deturbulator can significantly exceed best L/D and endurance of aggressive laminar flow wings.

Acknowledgments

The author would like to thank Richard H. Johnson conducting the flight tests and sharing the data. The flight tests were flown out of Caddo Mills, TX regional airport and funded by Dallas Gliding Association, who are also acknowledged. Acknowledgements are also due to Jim Hendrix, Oxford Aero Equipment, Oxford, MS for providing the test aircraft and identifying trends in the test data. Acknowledgements are also due to the National Science Foundation (SBIR Award IIP-0638157) for supporting the development of the Deturbulator.

References

[1] Simons, M., 2005, *Sailplanes 1965-2000*, 2nd Ed., EQUIP Werbung & Verlag GmbH, Königswinter, Germany.

[2] http://en.wikipedia.org/wiki/Glider

[3] Liebeck, R. H., "Design of Subsonic Airfoils for High Lift,"*Journal of Aircraft*, Vol. 15, No. 9, 1978, pp. 547-561.

[4] Sinha, S.K., "Aircraft Drag Reduction with Flexible Composite Surface Boundary Layer Control," (AIAA 2004-2121), 2nd. AIAA Flow Control Conference, 28 Jun-July 1 2004, Portland, OR.

[5] Sinha, S.K. and Ravande, S.V., "Drag Reduction of Natural Laminar Flow Airfoils with a Flexible Surface Deturbulator", AIAA Paper 2006-3030, 3rd. AIAA Flow Control Conference, San Francisco, CA, June 5-8, 2006.

[6] Sinha, S.K., and Ravande, S.V., "Sailplane Performance Improvement Using a Flexible Composite Surface Deturbulator," AIAA Paper 2006-0447, 44th AIAA Aerospace Sciences Meeting, Reno, NV, Jan 9-12, 2006.

[7] Sinha, S., and Sinha, S.K.,, "Method of Reducing Drag and Increasing Lift Due to Flow of a Fluid Over Solid Objects", International Patent Application No.: PCT/US2006/011430, International Publication Number WO 2006/105174 A2 with an International Publication Date of 5 October 2006.

[8] Sinha, S.K., "System and Method for Using a Flexible Composite Surface for Pressure-Drop Free Heat Transfer Enhancement and Flow Drag Reduction," U.S. Patent Application fied Jan 31, 2003, PCT Intl Patent Application filed Feb 3, 2003. (USPTO Pub. No. US-2003-0145980-A1, Aug 2003).

[9] Bushnell, D.M. and Hefner, J.M., "Effect of Compliant Wall on Turbulent Boundary Layers," *Physics of Fluids,* Vol. 20, No. 10., Pt II, Oct 1977, pp. s31-s48.

[10] Dixon, A.E., Lucey, A.D., and Carpenter, P.W., "Optimization of viscoelastic compliant walls for transition delay", *AIAA Journal*, **32**(2), pp.256-267, ISSN:0001-1452, (Feb 1994)

[11] Carpenter, P.W., Lucey, A.D., and Davies, C., "Progress on the use of compliant walls for laminar-flow control", *Journal of Aircraft*, **38**(3), pp.504-512, ISSN:0021-8669, (May 2001)

[12] Sinha, S.K.; "System for Efficient Control of Flow Separation using a Driven Flexible Wall," U.S. Patent No. 5,961,080, October 5, 1999.

[13] Pal, D and Sinha, S.,"Controlling Unsteady Separation on a Cylinder With a Driven Flexible Wall" *AIAA Journal*, Vol.36, No.6., 1998, pp. 1023-1028.

[14] Sinha, S.K.,., "Flow Separation Control with Microflexural Wall Vibrations," *Journal of Aircraft*, Vol.38, No.3., May-June-2001, pp. 496-503.

[15] Mangla, N.L., and Sinha, S.K., 2004, "Controlling Dynamic Stall with an Active Flexible Wall" AIAA Paper AIAA-2004-2325; 2nd AIAA Flow Control Conf, Portland, June 28-July 1, 2004.

[16] Schlichting, H. , 1979, *Boundary Layer Theory*, McGraw Hill, New York, NY.

[17] Tennekes, H., and Lumley, J.L., 1989, *A First Course in Turbulence*, The MIT Press, Cambridge, MA

[18] Sinha, S.K. and Sinha, S.L., "Improving Automotive Fuel Efficiency with Deturbulator Tape" (Paper #: 07APAC-15), Asia Pacific Automotive Engineering Conference, August 5-8, 2007, Hollywood, CA, USA, (to be presented).

[19] Johnson, R.H., 2007, "A Flight Test Evaluation of the Sinha Wing Performance Enhancing Deturbulators," SOARING and Motorgliding Magazine, The Journal of the Soaring Society of America Inc., Vol 71., No.5, May 2007, pp. 35-41.

[20] Drela, M., XFOIL: "An Analysis and Design System for Low Reynolds Number Airfoils (XFOIL 6.94, 18 December 2001)". *Low Reynolds Number Aerodynamics*, T. J.Mueller (ed.), Lecture Notes in Engineering, vol. 54, Springer-Verlag Berlin, 1989, pp.1–12.

[21] McCormick, B.W., 1995, *Aerodynamics Aeronautics and Flight Mechanics*, 2nd. Ed., John Wiley and Sons.